Spin-polarization observables of deuteron photodisintegration at low energies in pionless effective-field theory

Young-Ho Song,[1] Shung-Ichi Ando,[2] and Chang Ho Hyun[3,*]
[1]*Rare Isotope Science Project, Institute for Basic Science, Daejeon 34047, Korea*
[2]*School of Mechanical and ICT Convergence Engineering, Sunmoon University, Asan, Chungnam 31460, Korea*
[3]*Department of Physics Education, Daegu University, Gyeongsan 38453, Korea*
(Received 26 January 2017; published 13 July 2017)

Spin-polarization observables of deuteron photodisintegration at low energies are studied in a pionless effective-field theory up to next-to-next-to-leading order (NNLO). The total and differential cross sections, induced neutron polarization $P_{y'}$, and tensor analyzing powers T_{20} and T_{22} of the process are calculated at photon energies from the breakup threshold to 20 MeV. We find that the NNLO corrections in the cross sections and $P_{y'}$ converge well whereas they turn out to be important contributions in T_{20} and T_{22}. We discuss the discrepancy between theory and experiment in $P_{y'}$ still persisting as well as an implication of our result to the first measurement of T_{20} at low energies in the High Intensity Gamma-Ray Source facility at Duke University.

DOI: 10.1103/PhysRevC.96.014001

I. INTRODUCTION

Observables related to polarization provide more detailed information on nuclear reactions than the unpolarized ones [1]. There still remains a couple of problems which show discrepancy between experiment and theory even in few-nucleon systems at low energies [2–4]. Induced neutron polarization $P_{y'}$ of the photodisintegration of deuteron is an example and one can find more information in the HIGS2 proposal [5]. A proposal for the photodisintegration of deuteron at the High Intensity Gamma-Ray Source (HIGS) facility at Duke University is focusing on the role of the final state. Tensor analyzing power T_{20} is chosen for the investigation, which depends on the d state of the deuteron wave function as well as the polarization states. The main objective of the experiment is to figure out or resolve the discrepancy between experiment and theory at photon energies around 10 MeV, and obtain precise data for T_{20} which has not been measured yet in the low-energy regime.

Pionless effective-field theory (EFT) for low-energy phenomena, in which the pion can be treated as a heavy degree of freedom and integrated out of the effective Lagrangian, provides us a model independent and perturbative calculation method [6–8]. An effective Lagrangian of the pionless EFT can be constructed by using only the symmetry property of the system and momentum expansion in the low energy. The pionless EFT is able to successfully explain many low-energy properties of nuclear two-body systems with and without external electromagnetic probes [7–10]. Because the measured induced neutron polarization $P_{y'}$ in $\gamma + d \to \vec{n} + p$ and theoretical calculation using the phenomenological potential model show a discrepancy [2,4], it is desirable to have a model independent calculation.

In this paper, we compute the photodisintegration cross section of deuteron by using a pionless EFT in dibaryon formalism [8,11,12] up to next-to-next-to-leading order (NNLO) which includes sd wave mixing effects of the deuteron wave function. Dibaryon fields which have the quantum numbers of two-nucleon systems in either scattering or bound states are introduced to facilitate the resummation of effective range effects to infinite order. The details of formalism up to next-to-leading order (NLO) for the photodisintegration of deuteron have been reported in [4,8,13]. The result of pionless EFT up to NLO in [4] shows discrepancy with the experimental data of $P_{y'}$ [14], similar to the phenomenological nuclear force model calculations of [1,2], but the result is different from the potential model calculation with increasing photon energy. Even though the unpolarized cross sections could be well described up to NLO, the spin dependent observables can be sensitive to the higher-order corrections. The d state in the deuteron wave function could be properly accounted for when we increase the expansion up to NNLO. An NNLO calculation in the pionless EFT with dibaryon formalism for the electrodisintegration of deuteron has been reported by Christlmeier and Griesshammer [15]. Because the photodisintegration of deuteron has the same electromagnetic hadronic currents of the electrodisintegration of deuteron up to NNLO, we employ the expression of the hadronic currents reported in [15]. Thus, we calculate the total cross section, the differential cross section, $P_{y'}$, T_{20}, and T_{22} from threshold to 19.8 MeV in photon energy in the center-of-mass frame. We compare the results up to NNLO with those of NLO, and other theoretical results. Experimental data are compared when available.

The paper is organized as follows. In Sec. II we present basic formalism of the pionless EFT and the analytic forms of the transition amplitudes and probabilities. In Sec. III numerical results and related discussions are given. In Sec. IV we summarize the present paper.

II. FORMALISM

In this paper, we employ the standard counting rules of pionless EFT, in which the expansion parameter is typical momentum divided by pion mass and satisfies $Q \sim 1/3$ [6,7].

*hch@daegu.ac.kr

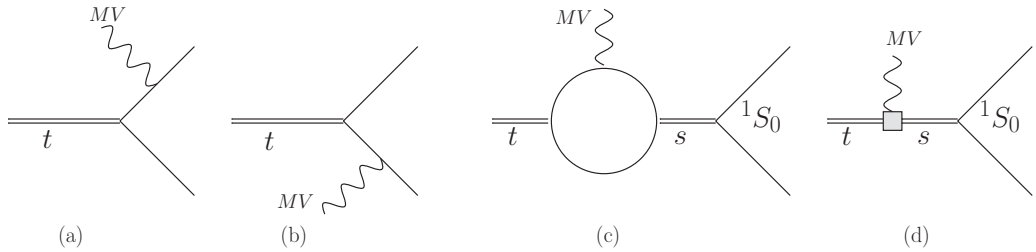

FIG. 1. Diagrams for LO (a–c) and NLO (d) of isovector magnetic currents (denoted as MV). The double line represents a dibaryon field of spin triplet (t) and singlet (s) states. The square in (d) represents the NLO L_1 term. Only $^1S_0$ final states contribute to the magnetic currents in (c, d) while (a, b) include spin singlet partial waves with $L = 0, 1, \ldots$.

In this section, we display the Lagrangian up to NNLO and the expression of the cross sections, and obtain the spin-polarization observables of the photodisintegration of deuteron.

A. Lagrangian

The effective Lagrangian in the pionless EFT up to NNLO can be written as [8]

$$\mathcal{L} = \mathcal{L}_N + \mathcal{L}_s + \mathcal{L}_t + \mathcal{L}_{\rm st}, \tag{1}$$

where $\mathcal{L}_N$ is a standard one-nucleon Lagrangian; $\mathcal{L}_s$ and $\mathcal{L}_t$ are Lagrangians for the two-nucleon part in the s-wave spin singlet and triplet channel, respectively; and $\mathcal{L}_{\rm st}$ is a Lagrangian for the spin mixing channel. Thus, one has

$$\mathcal{L}_N = N^\dagger\left[iD_0 + \frac{\vec{D}^2}{2M} + \frac{e}{2M}(\kappa_0 + \kappa_1\tau_3)\vec{\sigma}\cdot\vec{B}\right]N, \tag{2}$$

$$\mathcal{L}_s = -s_a^\dagger\left[iD_0 + \frac{\vec{D}^2}{4M} - \Delta_s\right]s_a - y_s\left[s_a^\dagger N^T P_a^{(^1S_0)} N + \text{H.c.}\right], \tag{3}$$

$$\mathcal{L}_t = -t_i^\dagger\left[iD_0 + \frac{\vec{D}^2}{4M} - \Delta_t\right]t_i - y_t\left[t_i^\dagger N^T P_i^{(^3S_1)} N + \text{H.c.}\right] - \frac{C_{\rm sd}}{\sqrt{M\rho_d}}\left[\delta_{ix}\delta_{jy} - \frac{1}{3}\delta_{ij}\delta_{xy}\right]\left[t_i^\dagger(N^T\mathcal{O}_{xy,j}N) + \text{H.c.}\right], \tag{4}$$

$$\mathcal{L}_{\rm st} = \frac{eL_1}{M\sqrt{r_0\rho_d}}[t_i^\dagger s_3 B_i + \text{H.c.}], \tag{5}$$

where N is the nonrelativistic nucleon field, and s_a and t_i are the dibaryon fields in the $^1S_0$ and $^3S_1$ states, respectively. The dibaryon fields couple with two nucleons in each partial wave or with other dibaryon fields. Spin projection operators, $P_a^{(^1S_0)}$ and $P_i^{(^3S_1)}$, for the s-wave spin singlet and triplet channels are given as

$$P_a^{(^1S_0)} = \frac{1}{\sqrt{8}}\sigma_2\tau_2\tau_a, \quad P_i^{(^3S_1)} = \frac{1}{\sqrt{8}}\sigma_2\sigma_i\tau_2, \tag{6}$$

where σ_i and τ_a are the Pauli matrices for spin and isospin spaces, respectively. The projection operators satisfy the normalization condition

$$\text{Tr}(P_j^\dagger P_k) = \tfrac{1}{2}\delta_{jk}. \tag{7}$$

In addition, a spin projection operator for the sd wave mixing channel is given as

$$\mathcal{O}_{xy,j} = -\tfrac{1}{4}\big(\overleftarrow{D}_x\overleftarrow{D}_y P_j^{(^3S_1)} + P_j^{(^3S_1)}\overrightarrow{D}_x\overrightarrow{D}_y - \overleftarrow{D}_x P_j^{(^3S_1)}\overrightarrow{D}_y - \overleftarrow{D}_y P_j^{(^3S_1)}\overrightarrow{D}_x\big), \tag{8}$$

where D_μ is a covariant derivative, given by $D_\mu = \partial_\mu + ieQ_{\rm em}A_\mu$ with a charge operator $Q_{\rm em}$, the electric charge e, and a photon field A_μ (and $\vec{B} = \vec{\nabla}\times\vec{A}$). Three parameters, M, κ_0, and κ_1, appear in the one-nucleon part of the Lagrangian: M is the nucleon mass, and κ_0 and κ_1 are magnetic momenta of the nucleon for isosinglet and isovector channels, respectively, $\kappa_0 = 0.44$ and $\kappa_1 = 2.35$. Six parameters, Δ_s, Δ_t, y_s, y_t, $C_{\rm sd}$, and L_1, appear in the two-nucleon part. The first four parameters are fixed by the effective range parameters: scattering length and effective range for each NN scattering channel. Thus, one has [8]

$$\Delta_s = \frac{2}{Mr_0}\left(\frac{1}{a_0} - \mu\right), \quad \Delta_t = \frac{2}{M\rho_d}\left(\gamma - \frac{\rho_d}{2}\gamma^2 - \mu\right),$$
$$y_s = \frac{\sqrt{8\pi}}{M\sqrt{r_0}}, \quad y_t = \frac{\sqrt{8\pi}}{M\sqrt{\rho_d}}, \tag{9}$$

where μ is a dimensional parameter from the power divergence subtraction regularization scheme of the loop diagrams [16].[1] a_0 and r_0 are the scattering length and effective range in the $^1S_0$ channel, $a_0 = -23.71$ fm and $r_0 = 2.73$ fm. γ is the deuteron binding momentum, $\gamma = \sqrt{MB} = 45.70$ MeV with the deuteron binding energy B, $B = 2.225$ MeV, and ρ_d is the effective range in the deuteron channel, $\rho_d = 1.764$ fm. The remaining two parameters, $C_{\rm sd}$ and L_1, are fixed by using asymptotic ratio $\eta_{\rm sd} = 0.0254$ of the s/d wave of the deuteron wave function and the thermal neutron capture cross section of the proton, respectively. We obtain $C_{\rm sd} = \frac{6\sqrt{\pi}\eta_{\rm sd}}{\sqrt{M\gamma^2}}$ and $L_1 = -4.41$ fm.

The amplitude $\mathcal{A}$ of photodisintegration, $\gamma + d \to n + p$, can be written as

$$\mathcal{A} = \epsilon_\mu^{(\gamma)}(q)J^\mu_{\rm hadr} \tag{10}$$

[1] In the calculation of loop integrals for hadronic currents in [15], the power divergence subtraction scheme is combined with dimensional integration in spatial dimensions after using contour integration for the energy part. For more details, one may refer to the Appendix in [15].

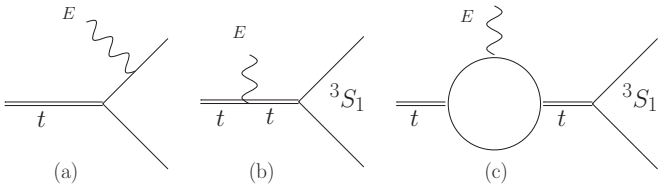

FIG. 2. Diagrams for LO electric currents. The double line represents a triplet dibaryon field. While only the $^3S_1$ final state contributes in (b, c), other partial-wave contributions are included in (a), which is dominated by the isovector $E1$ amplitude to final spin triplet P-wave states.

where $\epsilon_\mu^{(\gamma)}(q)$ is a polarization vector of the photon with four-momentum q, and $J^\mu_{\rm hadr}$ is a hadronic current. Hadronic current $J^\mu_{\rm hadr}$ is divided into electric and magnetic currents, $J^{(E)\mu}_{\rm hadr}$ and $J^{(M)\mu}_{\rm hadr}$, which are given as

$$J^{(E)\mu}_{\rm hadr} = i\frac{\sqrt{Z}}{\sqrt{8}}(N_p^\dagger\sigma^i\sigma_2 N_n^*)\epsilon^j_{(d)}J^\mu_{E,ij},$$
$$J^{(M)k}_{\rm hadr} = \frac{\sqrt{Z}}{\sqrt{8}}\epsilon^{ijk}\epsilon^i_{(d)}(N_p^\dagger\sigma_2 N_n^*)J^j_M, \quad (11)$$

where N_p and N_n are the Pauli spinors of the proton and neutron, and Z is a wave-function normalization factor of the deuteron, $Z = \frac{\gamma\rho_d}{1-\gamma\rho_d}$. Since the isoscalar magnetic moment is smaller than the isovector magnetic moment ($\kappa_0/\kappa_1 \lesssim Q$), isoscalar magnetic currents are treated as a numerically higher order in this paper and thus not included in the currents. The hadronic magnetic currents consist of contributions at leading order (LO) and NLO (see Fig. 1), while the electric currents have LO (see Fig. 2) and NNLO (see Fig. 3) contributions which come from the mixing of the s wave and d wave. The explicit expression of the hadronic currents in Eq. (11) can be found in the Appendix of [15].[2]

[2]Since no explicit multipole expansion is done and the plane wave is used for final nucleons, the currents in Eq. (11) contain various multipole amplitudes including dominant $M1$ and $E1$ amplitudes.

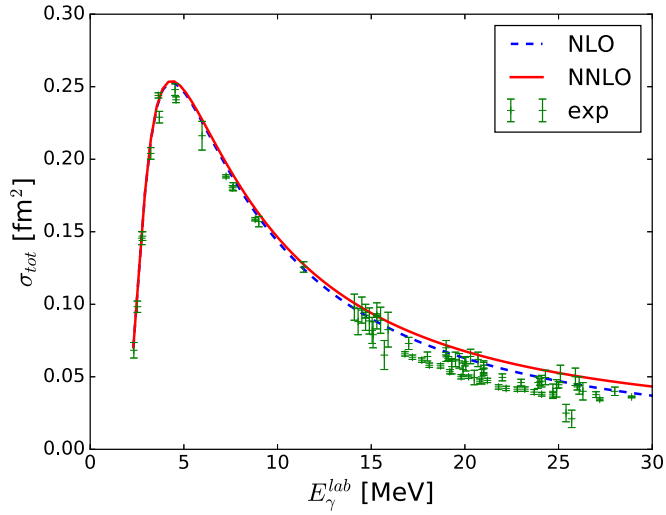

FIG. 4. Unpolarized total cross section $\sigma_{\rm tot}$ of deuteron photodisintegration up to NLO and NNLO. Experimental data [18–27] are also displayed in the figure.

B. Cross section and observables

An unpolarized differential cross section for the $\gamma + d \to n + p$ process is given in terms of an amplitude $\mathcal{A}_{m_n,m_p,\lambda,m_d}$ as

$$\frac{d\sigma_0}{d\Omega_p} = \frac{\alpha}{4\pi}\frac{p_p E_p}{E_\gamma}\frac{1}{2\cdot 3}\sum_{m_n,m_p,\lambda,m_d}\left|\mathcal{A}_{m_n,m_p,\lambda,m_d}\right|^2, \quad (12)$$

where λ denotes the polarization of the photon and m_d, m_n, and m_p are the deuteron, neutron, and proton spin projections, respectively. The unpolarized differential cross section in the center-of-mass frame with nonrelativistic approximation is obtained by summing the spin states. α is the fine-structure constant, and E_γ is the photon energy in the center-of-mass frame. The magnitude of three-momentum p_p and the energy E_p of the proton read

$$p_p = \frac{1}{2}\sqrt{\left(E_\gamma + \sqrt{M_d^2 + E_\gamma^2}\right)^2 - 4M^2}, \quad E_p = \sqrt{M^2 + p_p^2}, \quad (13)$$

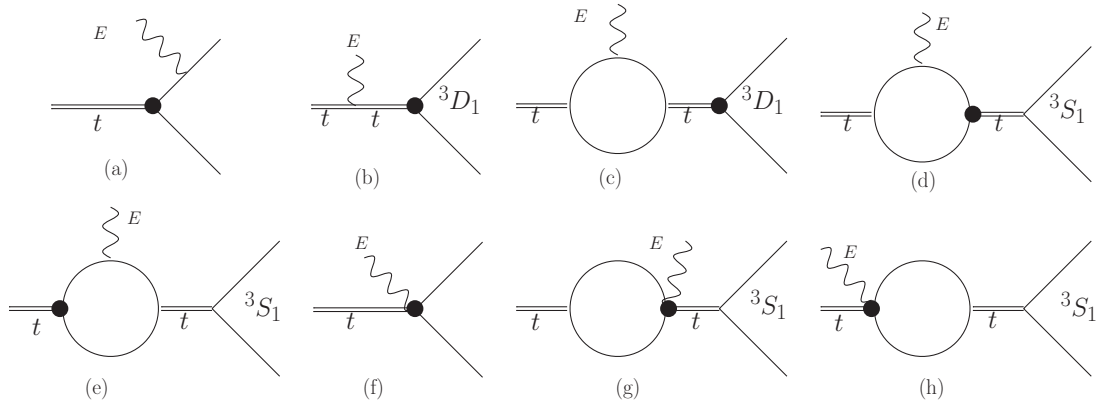

FIG. 3. Diagrams for NNLO electric currents (denoted as E). The double line represents a triplet dibaryon field. The black blob represents the sd mixing $C_{\rm sd}$ contribution. While only the $^3S_1$ final state contributes to (d, e, g, h) and only the $^3D_1$ final state contributes to (b, c), (a, f) include other spin triplet partial-wave contributions too.

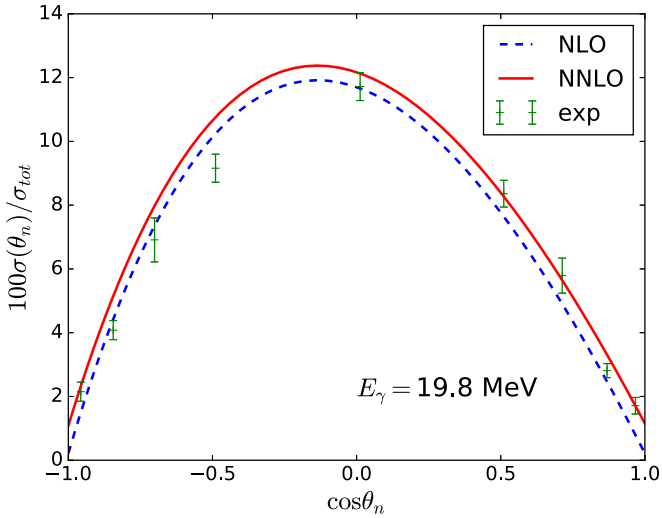

FIG. 5. Ratio of the unpolarized differential cross section and total cross section for the photon energy 19.8 MeV up to NLO (blue dashed) and NNLO (red solid). Experimental data [28] are also displayed.

where M_d is the deuteron mass. From now on, the spin indices of the amplitude will be implied for the amplitude $\mathcal{A}$ for convenience. Any spin dependent observables can be written in an appropriate combination of differential cross section $\frac{d\sigma}{d\Omega_p}(m_n, m_p, \lambda, m_d)$.

In this paper, we will focus on the spin-polarization observables: the induced polarization $P_{y'}$ of the neutron, and the tensor analyzing powers T_{20} and T_{22} in the deuteron photodisintegration. Let us choose the incoming photon momentum as z direction $\hat{q} = \hat{z}$, which is also a spin quantization axis, and then introduce a second reference frame $\hat{x}'$, $\hat{y}'$, and $\hat{z}'$ such that the direction of the outgoing neutron momentum is along the z' axis, $\hat{z}' = \hat{p}_n$, and $\hat{y}' \propto \hat{q} \times \hat{p}_n$ for convenience. In the form of components, $\hat{x}'$, $\hat{y}'$, and $\hat{z}'$ are represented as $(\cos\theta_n \cos\phi_n, \cos\theta_n \sin\phi_n, -\sin\theta_n)$, $(-\sin\phi_n, \cos\phi_n, 0)$, and $(\sin\theta_n \cos\phi_n, \sin\theta_n \sin\phi_n, \cos\theta_n)$, respectively. Thus, $P_{y'}$ is defined in terms of polarized differential cross sections:

$$P_{y'}(\theta_n) \equiv \frac{\sigma_{+y'}(\theta_n) - \sigma_{-y'}(\theta_n)}{\sigma_{+y'}(\theta_n) + \sigma_{-y'}(\theta_n)}, \tag{14}$$

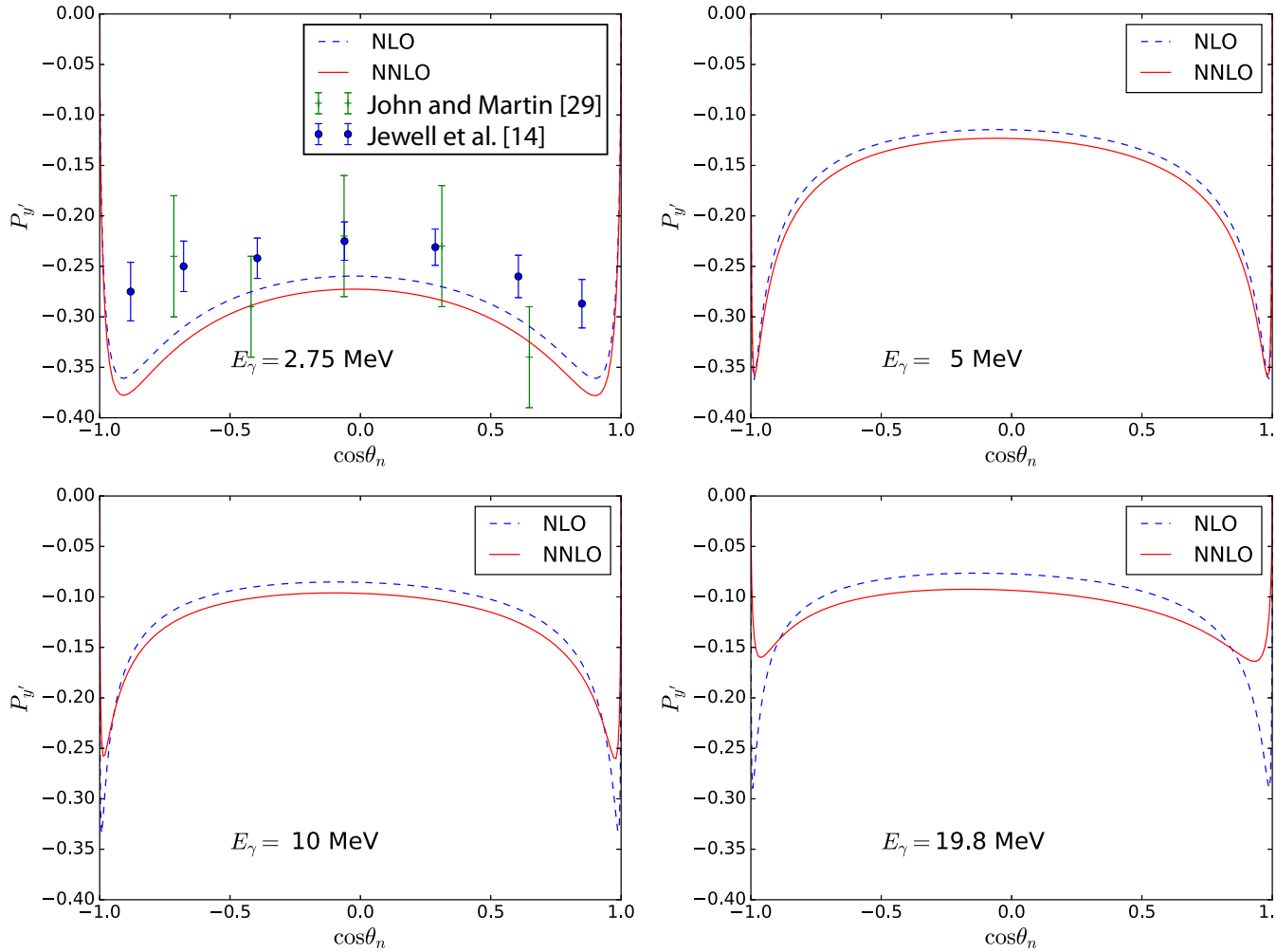

FIG. 6. $P_{y'}$ for the photon energies 2.75 MeV (top left), 5 MeV (top right), 10 MeV (bottom left), and 19.8 MeV (bottom right) up to NLO (blue dashed) and NNLO (red solid). Experimental data from John and Martin [29] and Jewell *et al.* [14] are included in the figure at $E_\gamma = 2.75$ MeV.

where $\sigma_{+y'}(\sigma_{-y'})$ is a differential cross section in which the spin of the outgoing neutron is parallel (antiparallel) to the $\hat{y}'$ direction.

The general form of the polarized deuteron cross section with unpolarized photons is given as [17]

$$\frac{d\sigma}{d\Omega} = \frac{d\sigma_0}{d\Omega}\Bigg[1 + \sum_{I=1,2} P_I^d \sum_{M\geqslant 0} T_{IM}(\theta) \times \cos\left(M(\phi_d - \phi) - \delta_{I1}\frac{\pi}{2}\right) d^I_{M0}(\theta_d)\Bigg], \quad (15)$$

where P_I^d and $T_{IM}(\theta)$ are orientation parameters and analyzing powers, respectively, for $I = 1,2$. (θ,ϕ) represents a direction of the outgoing proton, the deuteron is oriented in a direction (θ_d,ϕ_d), and d^I_{M0} is a rotation matrix. When a density matrix of the deuteron is diagonal in a quantization axis $\rho^d_{m'm} = p_m\delta_{m'm}$ where p_m is a probability of finding a deuteron with a spin projection m, orientation parameters P_I^d are related to p_m as

$$P_1^d = \sqrt{\frac{3}{2}}(p_1 - p_{-1}), \quad P_2^d = \sqrt{\frac{1}{2}}(1 - 3p_0). \quad (16)$$

From the rotation matrix, let us define polarized cross sections $d\sigma^{\odot}$ for the deuteron polarization axis orienting to $(\theta_d = \frac{\pi}{2},\phi_d = 0)$, $d\sigma^{\uparrow}$ for that orienting to $(\theta_d = \frac{\pi}{2},\phi_d = \frac{\pi}{2})$, and $d\sigma^{\downarrow}$ for that orienting to $(\theta_d = \frac{\pi}{2},\phi_d = -\frac{\pi}{2})$. Thus, we have

$$\begin{aligned}
\frac{d\sigma^z}{d\Omega} &\equiv \frac{d\sigma_0}{d\Omega}\left[1 + P_2^d T_{20}(\theta)\right],\\
\frac{d\sigma^{\odot}}{d\Omega} &\equiv \frac{d\sigma_0}{d\Omega}\left[1 + P_2^d T_{22}(\theta)\sqrt{\frac{3}{8}} + P_2^d T_{20}(\theta)\left(-\frac{1}{2}\right)\right],\\
\frac{d\sigma^{\uparrow,\downarrow}}{d\Omega} &\equiv \frac{d\sigma_0}{d\Omega}\Bigg[1 + P_1^d T_{11}(\theta)\left(\mp\frac{1}{\sqrt{2}}\right) + P_2^d T_{22}(\theta)\\
&\quad\times\left(-\sqrt{\frac{3}{8}}\right) + P_2^d T_{20}(\theta)\left(-\frac{1}{2}\right)\Bigg]. \quad (17)
\end{aligned}$$

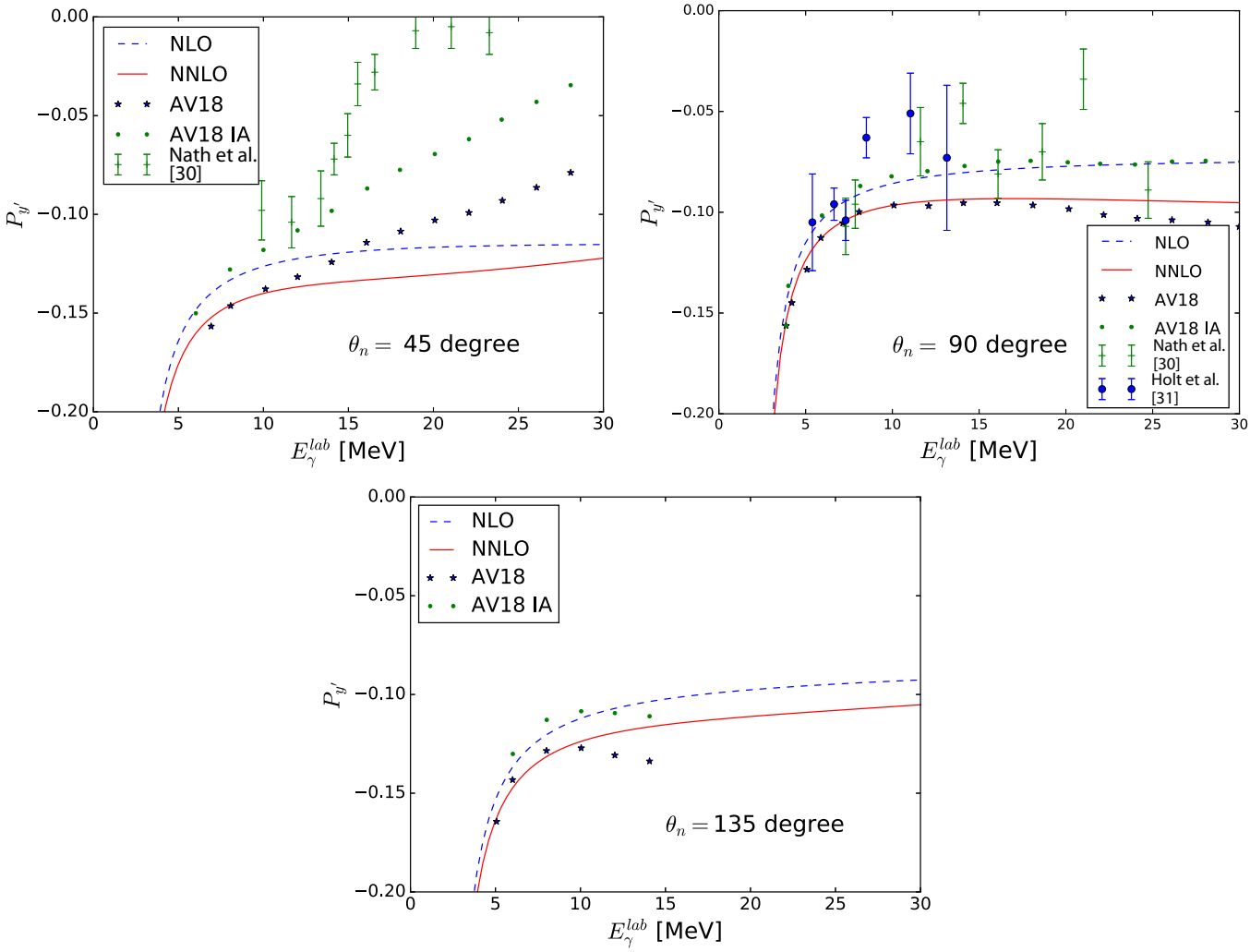

FIG. 7. $P_{y'}$ at three different angles with increasing photon energy up to NLO (blue dashed) and NNLO (red solid). Top left: $\theta_n = 45^\circ$. Top right: $\theta_n = 90^\circ$. Bottom: $\theta_n = 135^\circ$. Experimental results from Nath *et al.* [30] and Holt *et al.* [31] are also displayed in the figures at $\theta_n = 45$ and 90°.

The tensor analyzing powers, thus, can be obtained from the polarized cross sections as

$$T_{11} = \frac{1}{\sqrt{2}P_1^d}\frac{d\sigma^{\uparrow-\downarrow}}{d\sigma^0},$$
$$T_{20} = \frac{1}{P_2^d}\left(2 - \frac{d\sigma^{\odot} + \frac{1}{2}d\sigma^{\uparrow+\downarrow}}{d\sigma^0}\right) = \frac{1}{P_2^d}\left(\frac{d\sigma^z}{d\sigma_0} - 1\right),$$
$$T_{22} = \frac{\sqrt{2}}{\sqrt{3}P_2^d}\frac{d\sigma^{\odot} - \frac{1}{2}d\sigma^{\uparrow+\downarrow}}{d\sigma^0}, \tag{18}$$

where $d\sigma^{\uparrow\pm\downarrow} = d\sigma^{\uparrow} \pm d\sigma^{\downarrow}$. By choosing $p_1 = 1$, we have $P_1^d = \sqrt{\frac{3}{2}}$ and $P_2^d = 1/\sqrt{2}$. This corresponds to the choice of $\vec{\epsilon}_{(d)}$ in Eq. (11) such that $\vec{\epsilon}_{(d)} = -\frac{1}{\sqrt{2}}(0, +i, -1)$ for $d\sigma^{\odot}$, $\vec{\epsilon}_{(d)} = -\frac{1}{\sqrt{2}}(-i, 0, -1)$ for $d\sigma^{\uparrow}$, $\vec{\epsilon}_{(d)} = -\frac{1}{\sqrt{2}}(+i, 0, -1)$ for $d\sigma^{\downarrow}$, and $\vec{\epsilon}_{(d)} = -\frac{1}{\sqrt{2}}(1, +i, 0)$ for $d\sigma^z$.

III. NUMERICAL RESULT AND DISCUSSION

A. Total and differential cross sections

In Fig. 4, we plot curves of the total cross section calculated up to NLO and NNLO and include experimental data [18–27] as well. With the parameters fixed to low-energy data, the curves up to NLO and NNLO give the results consistent with the data to $E_\gamma^{\rm lab} = 30$ MeV. The correction from NNLO is about 10% of the contribution up to NLO at $E_\gamma^{\rm lab} \sim 20$ MeV, and about 20% at $E_\gamma^{\rm lab} \sim 30$ MeV. Although the total cross section turns out to be in good agreement with the experimental data up to relatively high energy, in principle, the pionless theory must be applied to the photon energies below 10 MeV, which corresponds to nucleon momentum close to the pion mass. Thus, in this paper, we limit the photon energy to the range $E_\gamma^{\rm lab} \leqslant 20$ MeV in the study of the spin observables.

In Fig. 5, curves of the unpolarized differential cross section divided by the total cross section at $E_\gamma = 19.8$ MeV are plotted by using our results up to NLO and NNLO, and the experimental data are also included [28]. Similar to the total cross section, the difference between NLO and NNLO is

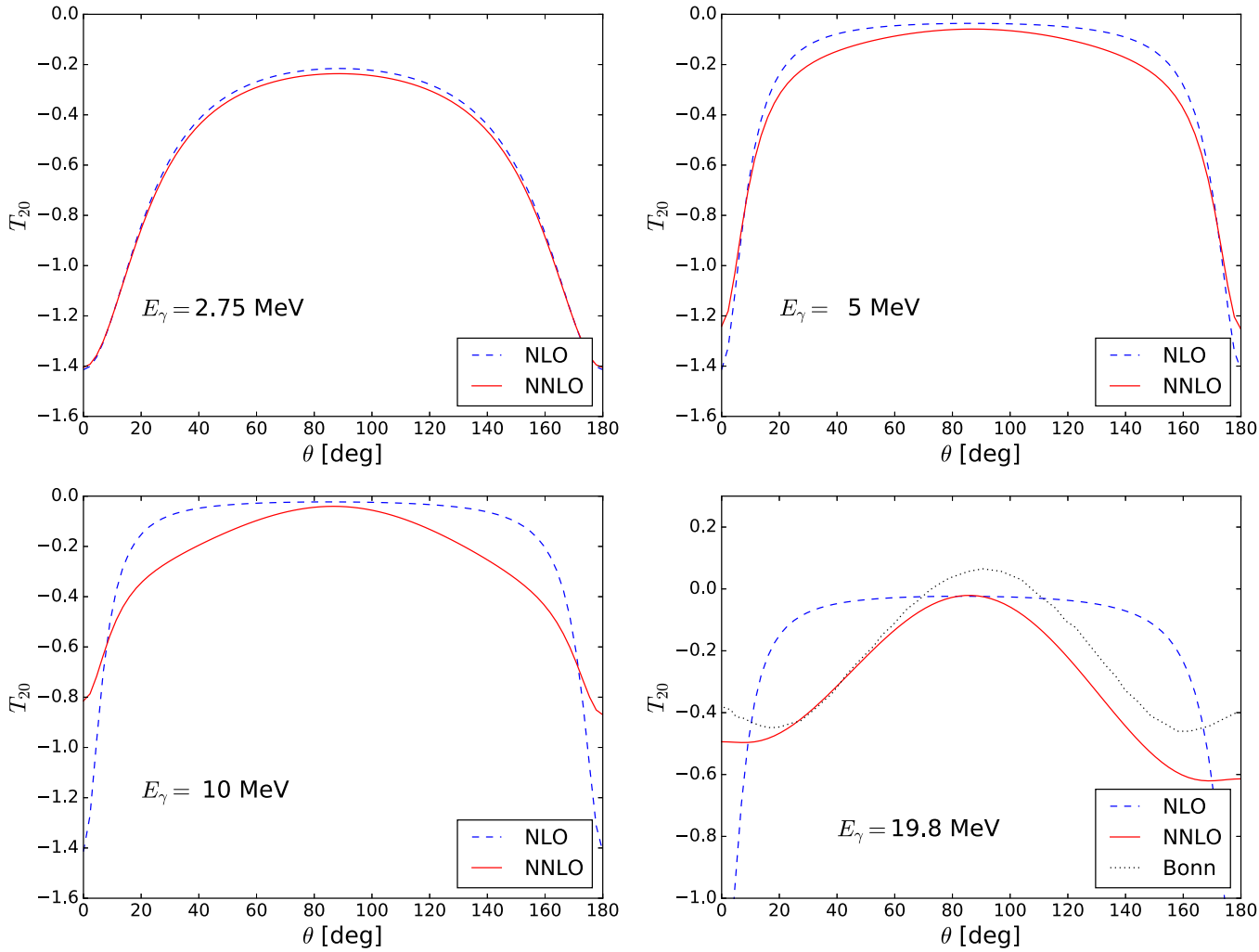

FIG. 8. T_{20} for the photon energies 2.75 MeV (top left), 5 MeV (top right), 10 MeV (bottom left), and 19.8 MeV (bottom right) up to NLO (blue dashed) and NNLO (red solid). The Bonn potential result is from [1] (black dotted).

negligible up to 10 MeV, and the NNLO correction converges well even at $E_\gamma = 19.8$ MeV.

B. Induced neutron polarization $P_{y'}$

In Fig. 6, our results of $P_{y'}$ up to NLO and NNLO at $E_\gamma = 2.75$, 5, 10, and 19.8 MeV are plotted as functions of $\cos\theta_n$, where θ_n is the angle for the outgoing neutron in the center-of-mass frame. Experimental data from John and Martin [29] and Jewell *et al.* [14] at $E_\gamma = 2.75$ MeV are also included in the figure. We find that the NNLO corrections converge well at all the photon energies and are small compared to those up to NLO. Discrepancy between theory and experiment of $P_{y'}$ at $E_\gamma = 2.75$ MeV, which has been reported in our previous work in the pionless EFT up to NLO [4], cannot be resolved by including the NNLO corrections.

Figure 7 shows the results of $P_{y'}$ in three different angles with increasing photon energy. The pionless EFT results up to NLO and NNLO agree well with phenomenological potential model calculation of Av18 in impulse approximation and Av18 calculation with exchange currents [2] at low energies, respectively. The agreement implies that model independent calculation of pionless EFT supports the Av18 results rather than the measurement by Nath *et al.* [30]. The results of Av18 and pionless EFT converge up to $E_\gamma \sim 10$ MeV, and start to deviate for $\theta_n = 45$ and 135°, while $\theta_n = 90°$ results show good agreement even at $E_\gamma \geqslant 10$ MeV. This could be related to higher-order corrections which are neglected in the present paper.

C. Tensor analyzing power T_{20} and T_{22}

By computing differential cross sections, $d\sigma^{\odot}$, $d\sigma^{\uparrow}$, and $d\sigma^{\downarrow}$, we can obtain the tensor analyzing powers T_{11}, T_{20}, and T_{22}. However, because $d\sigma^{\uparrow} \simeq d\sigma^{\downarrow}$ up to NNLO, we obtain $T_{11} \simeq 0$. We would need to include higher-order corrections to have a sizable contribution to T_{11}. Also, T_{22} is dominated by the NNLO contribution since $T_{22} \simeq 0$ at NLO, which implies that a contribution to T_{22} mostly comes from the sd mixing effects.

In Fig. 8, we summarize our results of T_{20} at NLO and NNLO. There are interesting behaviors absent or appearing weakly in other observables. First of all, in the observables considered so far, the results of NNLO are almost identical to

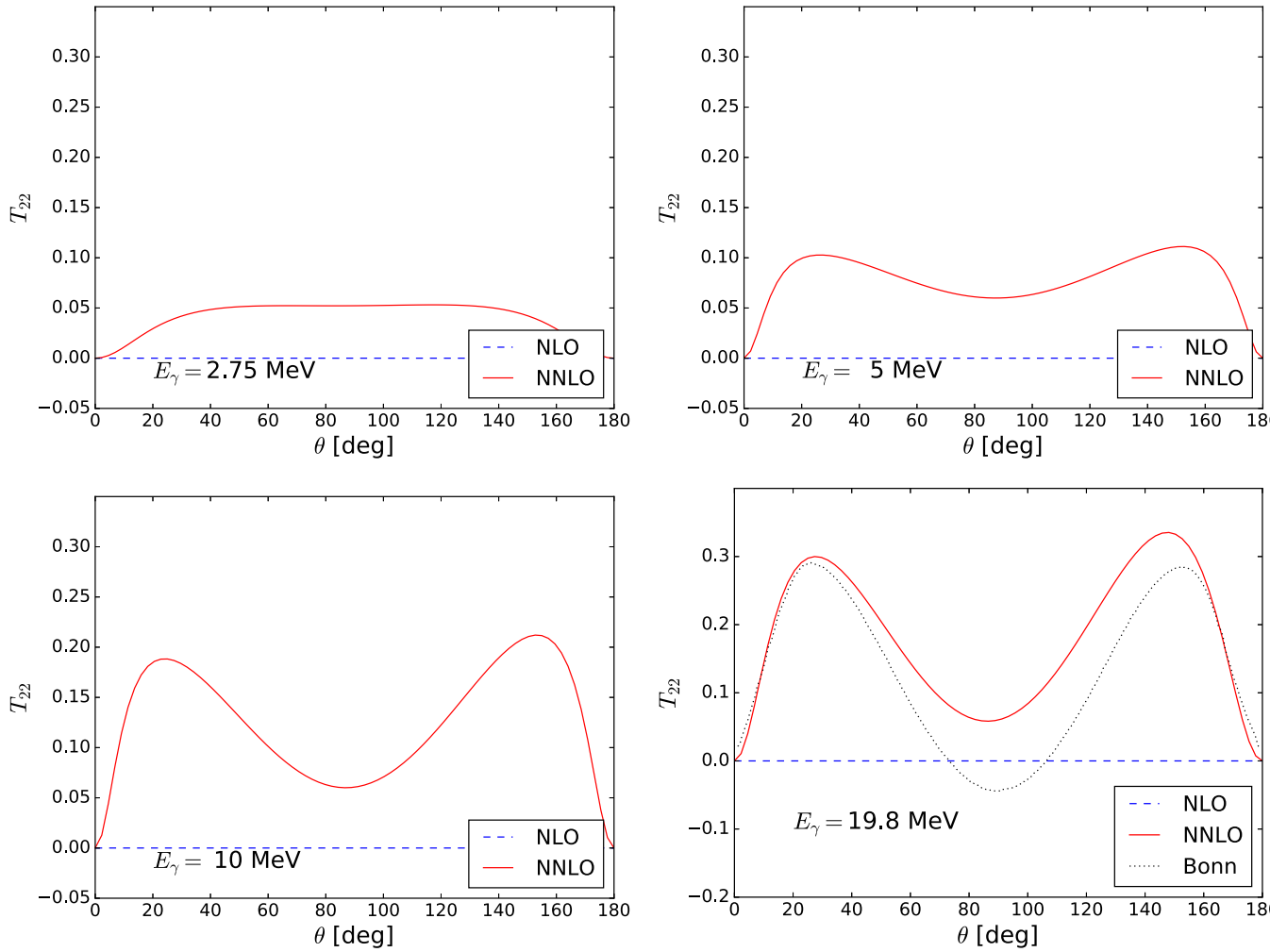

FIG. 9. T_{22} for the photon energies 2.75 MeV (top left), 5 MeV (top right), 10 MeV (bottom left), and 19.8 MeV (bottom right) up to NLO (blue dashed) and NNLO (red solid). The Bonn potential result is from [1] (black dotted).

those of NLO up to $E_\gamma = 10$ MeV, but for T_{20} a non-negligible difference appears already at $E_\gamma = 5$ MeV. As the energy increases, the NLO result becomes the shape of a flat and wide plateau. The value of T_{20} in the flat region is close to zero and independent of the energy. Similarly the values at $\theta = 0$ and 180° remain the same regardless of the energy.

The result at $E_\gamma = 19.8$ MeV is similar to the results obtained from the Bonn potential model calculations, lying between "N+MEC+IC" and "N+MEC+IC+RC" in Fig. 7.4.13 in [1]. The effect of NNLO can be distinguished from that of NLO even at $E_\gamma = 10$ MeV, which is the energy of interest in the HIGS proposal [5]. Therefore measurement of T_{20} will provide a unique opportunity to test the role of higher orders in the pionless theory. At the same time, it might help to understand the origin of the discrepancy between experiment and theory in the polarization observables in few-body systems.

In Fig. 9, curves of T_{22} up to NLO and NNLO at $E_\gamma = 2.75$, 5, 10, and 19.8 MeV are plotted as functions of θ. As mentioned before, there is no contribution from the NLO corrections, and the NNLO corrections, mainly the sd wave mixing term, are a leading contribution to T_{22} at the low energies. Our result at $E_\gamma = 19.8$ MeV is compared to a result of the Bonn potential model [1]. One can see quantitative agreement between the NNLO result and the Bonn potential one.

IV. SUMMARY

Motivated by the proposal of measurement of the tensor analyzing power T_{20} at the HIGS facility, we studied the photodisintegration of deuteron at low energies. Pionless EFT with dibaryon fields is used as the tool for calculation, and corrections up to NNLO are included. Various observables such as the total and differential cross sections and spin dependent observables are investigated.

For the quantities that have nonvanishing contributions from LO such as the cross sections and $P_{y'}$, NNLO terms give perturbative corrections to the NLO results, and thus the theory shows good convergent behavior. For $P_{y'}$, including NNLO contributions, our result becomes closer to a sophisticated calculation with the Av18 model. The discrepancy between measurement and the NLO result remains unsolved even if we include the NNLO corrections.

For T_{20}, NNLO gives negligible change to the NLO result at $E_\gamma = 2.75$ MeV, but the correction becomes more significant as the energy increases. No data are available below 19.8 MeV, and we can make comparison to the result with the Bonn potential model at $E_\gamma = 19.8$ MeV. The agreement to the Bonn model result depends on the angle, but as a whole the NNLO result agrees well with that of the Bonn model quantitatively.

For T_{22}, contributions up to NLO are null, and nonvanishing values appear at NNLO. The NNLO result agrees with the Bonn model result fairly well. The agreement in the tensor analyzing power proves that increase of the order in both wave functions and operators for the external probe in the pionless EFT can give results as accurate as those of the most elaborate calculation with modern phenomenological potential models. Since our paper includes electric and magnetic hadronic currents up to NNLO, it would be interesting to check the effects of other multipole operators.

ACKNOWLEDGMENTS

We are grateful to Pil-Neyo Seo for stimulating discussion and for providing us information on the measurement of T_{20}. Y.H.S. and S.I.A. thank the Institute for Nuclear Theory at the University of Washington for its hospitality during the Program INT-16-1, "Nuclear Physics from Lattice QCD," where the present paper was started. The work of Y.H.S. was supported by the Rare Isotope Science Project of the Institute for Basic Science funded by Ministry of Science, ICT, and Future Planning and by National Research Foundation of Korea (Grant No. 2013M7A1A1075764). The work of S.I.A. was supported by the Basic Science Research Program through the National Research Foundation of Korea funded by the Ministry of Education of Korea (Grants No. NRF-2016R1D1A1B03930122 and No. NRF-2016K1A3A7A09005580).

[1] H. Arenhovel and M. Sanzone, Few-Body Syst. Suppl. **3**, 1 (1991).
[2] R. Schiavilla, Phys. Rev. C **72**, 034001 (2005).
[3] V. I. Kukulin, I. T. Obukhovsky, V. N. Pomerantsev, A. Faessler, and P. Grabmayr, Phys. Rev. C **77**, 041001 (2008).
[4] S. I. Ando, Y. H. Song, C. H. Hyun, and K. Kubodera, Phys. Rev. C **83**, 064002 (2011).
[5] P.-N. Seo (private communication, 2016).
[6] P. F. Bedaque and U. van Kolck, Annu. Rev. Nucl. Part. Sci. **52**, 339 (2002).
[7] J.-W. Chen, G. Rupak, and M. J. Savage, Nucl. Phys. A **653**, 386 (1999).
[8] S.-I. Ando and C. H. Hyun, Phys. Rev. C **72**, 014008 (2005).
[9] G. Rupak, Nucl. Phys. A **678**, 405 (2000).
[10] S. Ando, R. H. Cyburt, S. W. Hong, and C. H. Hyun, Phys. Rev. C **74**, 025809 (2006).
[11] D. B. Kaplan, Nucl. Phys. B **494**, 471 (1997).
[12] S. R. Beane and M. J. Savage, Nucl. Phys. A **694**, 511 (2001).
[13] Y. H. Song, C. H. Hyun, S. I. Ando, and K. Kubodera, Few-Body Syst. **54**, 371 (2013).
[14] R. W. Jewell, W. John, J. E. Sherwood, and D. H. White, Phys. Rev. **139**, B71 (1965).
[15] S. Christlmeier and H. W. Griesshammer, Phys. Rev. C **77**, 064001 (2008).
[16] D. B. Kaplan, M. J. Savage, and M. B. Wise, Phys. Lett. B **424**, 390 (1998).
[17] H. Arenhovel, Int. J. Mod. Phys. E **18**, 1226 (2009).
[18] R. Bernabei, A. Chisholm, S. d'Angelo, M. P. DePascale, P. Picozza, C. Schaerf, P. Belli, L. Casano, A. Incicchitti, D. Prosperi, and B. Girolami, Phys. Rev. C **38**, 1990 (1988).
[19] R. Moreh, T. J. Kennett, and W. V. Prestwich, Phys. Rev. C **39**, 1247 (1989); **40**, 1548(E) (1989).
[20] R. Bernabei, A. Incicchitti, M. Mattioli, P. Picozza, D. Prosperi, L. Casano, S. dAngelo, M. P. DePascale, C. Schaerf,

G. Giordano, G. Matone, S. Frullani, and B. Girolami, Phys. Rev. Lett. **57**, 1542 (1986).
[21] D. M. Skopik, Y. M. Shin, M. C. Phenneger, and J. J. Murphy, Phys. Rev. C **9**, 531 (1974).
[22] J. Ahrens, H. B. Eppler, H. Gimm, M. Kröning, P. Riehn, H. Wäffler, A. Zieger, and B. Ziegler, Phys. Lett. B **52**, 49 (1974).
[23] J. E. E. Baglin, R. W. Carr, E. J. Bentz, and C. P. Wu, Nucl. Phys. A **201**, 593 (1973).
[24] K. Y. Hara, H. Utsunomiya, S. Goko, H. Akimune, T. Yamagata, M. Ohta, H. Toyokawa, K. Kudo, A. Uritani, Y. Shibata, Y. W. Lui, and H. Ohgaki, Phys. Rev. D **68**, 072001 (2003).
[25] T. Shima, S. Naito, Y. Nagai, T. Baba, K. Tamura, T. Takahashi, T. Kii, H. Ohgaki, and H. Toyokawa, Phys. Rev. C **72**, 044004 (2005).
[26] Y. Birenbaum, S. Kahane, and R. Moreh, Phys. Rev. C **32**, 1825 (1985).
[27] H. Utsunomiya, S. Katayama, I. Gheorghe, S. Imai, H. Yamaguchi, D. Kahl, Y. Sakaguchi, T. Shima, K. Takahisa, and S. Miyamoto, Phys. Rev. C **92**, 064323 (2015).
[28] M. P. DePascale, G. Giordano, G. Matone, D. Babusci, R. Bernabei, O. M. Bilaniuk, L. Casano, S. dAngelo, M. Mattioli, P. Picozza, D. Prosperi, C. Schaerf, S. Frullani, and B. Girolami, Phys. Rev. C **32**, 1830 (1985).
[29] W. John and F. V. Martin, Phys. Rev. **124**, 830 (1961).
[30] R. Nath, F. W. K. Firk, and H. L. Schultz, Nucl. Phys. A **194**, 49 (1972).
[31] R. J. Holt, K. Stephenson, and J. R. Specht, Phys. Rev. Lett. **50**, 577 (1983).